Sudan University of Science and Technology

College of Graduate Studies

Effect of Thermal Treatments on Magnetic Properties of Some Magnetite Samples Investigated by ^{57}Fe Mössbauer Spectroscopy

أثر المعالجات الحرارية على الخصائص المغناطيسية لبعض عينات المغنتايت المتحقق منها بواسطة مطيافية موسباور ^{57}Fe

A Dissertation Submitted in Partial Fulfilment for the Requirement of a Master Degree (M. Sc) in Physics

By

Huda Osama Abd-ellatif

Supervisor

Dr. Nadir S.E. Osman

August 2018

الآية

قال تعالى

"أَمَّنْ هُوَ قَانِتٌ آنَاءَ اللَّيْلِ سَاجِدًا وَقَائِمًا يَحْذَرُ الْآخِرَةَ وَيَرْجُو رَحْمَةَ رَبِّهِ ۗ قُلْ هَلْ يَسْتَوِي الَّذِينَ يَعْلَمُونَ وَالَّذِينَ لَا يَعْلَمُونَ ۗ إِنَّمَا يَتَذَكَّرُ أُولُو الْأَلْبَابِ"

سورة الزمر آية 9

Dedication

I dedicate this dissertation to my parents Osama El-Dabi and Harm Shikhna who did not only raised and nurtured me but also taxed themselves dearly over the years for my education, happiness and drawing smile on my face. They have been a source of motivation and strength during every moment of despair and discouragement. Allah blesses their health and happiness.

Acknowledgements

I would like to thank Allah for all blessing he gave to my life, health and time to complete this work. Thanks to Sudan University of Science and Technology.

All thanks and appreciation to my supervisor Dr. Nadir Shams Eldin Osman for his patience and time, who gave me useful advices and support by encouraged me throughout this time. All thanks to University of KwaZulu-Natal, Westville campus for the Mössbauer measurements.

I thank my parents for being there to make me stronger than I would be without them.

Abstract

^{57}Fe Mössbauer spectroscopy is one of the most powerful tools that used in studying magnetic properties of materials. This work aims to investigate the magnetic properties of $Mg_xSr_xMn_xCo_{1-3x}Fe_2O_4$ (x = 0, 0.1, 0.2, 0.3 and 0.33) nanoparticles annealed at 500 ˚C. The aim extends to study the magnetic properties of $BaFe_2O_4$ sample as a function of different measuring temperatures. The results showed that magnetic hyperfine fields of the annealed samples were larger compared to as-prepared samples which agrees with literature. This reflects the effect of particle sizes on relaxation time τ as explained by Néel theory. The values of isomer shift were in the range of 0.30 to 0.51 mm/s. This indicates presence of Fe^{3+} ions in the samples. The line widths decreased in annealed samples compared to as-prepared ones.

Investigation the magnetic properties of $BaFe_2O_4$ sample as a function of different measuring temperatures of 77, 80, 90, 160, 200, 250 and 300 K revealed that increasing of measuring temperature changed the ferrimagnetic order of the sample to paramagnetic state. Isomer shift values were in the range of 0.30 to 0.45 mm/s, which related to Fe^{3+} ions. Line width values show no significant trends with increasing measuring temperatures.

The results showed that temperature (annealing or measuring) has significant influence upon hyperfine parameters therefore; it can decide the magnetic state of a material.

المستخلص

مطياف موسباور ^{57}Fe من أقوى الادوات المستخدمة في دراسة الخصائص المغناطيسية للمواد. يهدف هذا البحث للتحقق من الخصائص المغناطيسية باستخدام مطياف موسباور ^{57}Fe للمركب النانوي $Mg_xSr_xMn_xCo_{1-3x}Fe_2O_4$ (x = 0, 0.1, 0.2, 0.3, 0.33) المعالج حراريا في 500 درجة مئوية. أيضا يمتد هذا البحث لدراسة الخصائص المغناطيسية للمركب $BaFe_2O_4$ كدالة في درجات الحرارة المختلفة. نتائج المجال المغناطيسي الداخلي للعينات المعالجة حراريا أكبر مقارنة بقيم العينات قبل المعالجة الحرارية والتي درست سابقا، هذا يعكس تأثير زيادة حجم الجسيمات على زمن الاسترخاء τ كما وضحت نظرية نييل. قيم الازاحة الايزومرية تراوحت من 0.30 الى 0.51 ملم/ث، هذا يعزى لوجود أيونات الحديد Fe^{3+} في العينة. لوحظ نقصان قيم اتساع الخط في العينات المعالجة حراريا مقارنة بالعينات الغير معالجة حراريا.

التحقق من الخصائص المغناطيسية للعينة $BaFe_2O_4$ في درجات الحرارة (77, 80, 90, 160, 200, 250, 300 كلفن) يظهر أن زيادة درجات الحرارة تؤدي لتغيير حالة المادة من فيريمغنطيسية الى بارامغناطيسية. قيم الازاحة الايزومرية في مدى 0.30 – 0.45 ملم/ ث. والتي تتعلق بأيونات Fe^{3+} في العينة. لا تُظهر قيم اتساع الخط اتجاهات مهمة مع تزايد درجات الحرارة.

توضح هذه النتائج أن درجة الحرارة (معالجة حرارية أوقياس) لها تأثير على المعاملات المغناطيسية و التي يمكن أن تحدد الحالة المغناطيسية للمادة.

Table of Contents

الآية I

Dedication II

Acknowledgements III

Abstract IV

المستخلص V

Table of Contents VI

List of Figures VIII

List of Tables X

Chapter One

Introduction

1.1 Overview 1

1.1.2 Mössbauer effect 1

1.1.3 Doppler effect 3

1.1.4 Mössbauer applications 3

1.1.5 Magnetic materials 4

1.1.5.1 Diamagnetic 4

1.1.5.2 Paramagnetic 5

1.1.5.3 Ferromagnetic 5

1.1.5.4 Ferrimagnetic 5

1.1.5.5 Anti-ferromagnetic 5

1.1.6 Ferrites 6

1.1.6.1 Spinel ferrites 6

1.2 Literature reviews 7

1.3 Research problem 8

1.4 Research objectives 8

1.5 Dissertation layout 8

Chapter Two

Theoretical Background

2.1 Decay of ^{57}Co isotopes 10
2.2 Line width 11
2.3 Recoil-free fraction 11
2.4 Hyperfine interaction 12
2.4.1 Isomer shift 12
2.4.2 Magnetic hyperfine interaction 13
2.4.3Quadrupole splitting 15

Chapter Three

Experimental Details

3.2 Mössbauer drive system 17
3.3 The Mössbauer source 18
3.4 Mössbauer detector 18
3.5 Recording the Mössbauer spectrum 19
3.6 Mössbauer measurement procedures for the studied samples 20

Chapter Four

Results and Discussion

4.2 Magnetic properties of the annealed $Mg_xSr_xMn_xCo_{1-3x}Fe_2O_4$ nanoparticles ferrites .. 23
4.3 Analysis of Mössbauer spectra for $BaFe_2O_4$ sample as a function of measuring temperatures 27
4.3 Conclusions 31
4.4 Recommendations 31
4.5 Future Work 32
References 33

List of Figures

Figure 1.1. Recoilless emission and resonance absorption of γ-rays..…….....2

Figure 1.2. Mössbauer isotopes highlighted in red…….....3

Figure 1.3. Spinel structure, B atoms in octahedral sites and A atoms in octahedral sites…….....6

Figure 2.1. Recoil energy loss in free atoms……..…….....10

Figure 2.2. Schematic demonstration of ^{57}Co nuclear decay…….....11

Figure 2.3. Isomer shift in nuclear state……..…….....14

Figure 2.4. Effect of the magnetic dipole interaction in^{57}Fe Mössbauer spectrum…….....15

Figure 2.5. Effect of the electric quadrupole interaction leads to splitting in Mössbauer spectrum…….17

Figure 3.1. Schematic diagrammatic of Mössbauer spectrometer…….....20

Figure 3.2. Mössbauer spectrometer cryostat…….....22

Figure 3.3. Front setup of Mössbauer spectrometer.....….....23

Figure 4.1. Mössbauer spectra for $Mg_xSr_xMn_xCo_{1-3x}Fe_2O_4$ nanoferite samples annealed at 500 ^oC…….....26

Figure 4.2. Magnetic hyperfine fields values of $Mg_xSr_xMn_xCo_{1-3x}$ Fe_2O_4 (x = 0, 0.1, 0.2, 0.3, 0.33) annealed at 500 ^oC compared to as-prepared sample…….....27

Figure 4.3. Mössbauer spectra as a function of measuring temperature for $BaFe_2O_4$ sample…….....…29

Figure 4.4. Magnetic hyperfine fields as a function of measuring temperature…….....….31

List of Tables

Table 4.1. Isomer shifts (δ), hyperfine magnetic fields (H), line widths (Γ) and Fe^{+3} fraction population (f) on A- and B- sites for $Mg_xSr_xMn_xCo_{1-3x}Fe_2O_4$ samples annealed at 500 ^oC.....27

Table 4.2. Isomer shifts (δ), hyperfine magnetic fields (H), line widths (Γ) and Fe^{+3}fraction population (f) on A- and B- sites for $BaFe_2O_4$ as a function of measuring temperature…….....30

Chapter One

Introduction

Chapter One

Introduction

1.1 Overview

Interaction of electromagnetic radiation with matter is technologically important for many applications relates to remote sensing techniques. This interaction is associated with absorption, emission and scattering of electromagnetic radiation by atoms or molecules giving significant information about structure properties of matter (Kakkar, 2015). Spectroscopy which describes the interaction between electromagnetic radiation with matter has different types include X-rays photoelectron (XP), Infrared absorption (IR), Ultraviolet and visible absorption (UV-VIS), Nuclear magnetic resonance (NMR), Raman and Mössbauer spectroscopy.

1.1.2 Mössbauer effect

In 1957 Rudolf L. Mössbauer, while working on his doctoral thesis discovered the recoilless nuclear resonance absorption of γ-rays which known recently as Mössbauer effect (Philipp Gütlich, 1978). This has been observed for many elements which lead to significant contribution to physical, chemical, biological and earth sciences.

A γ-rays that emitted during the transition of an excited nucleus to the ground state, can be resonantly absorbed by another nucleus of the same nuclide, if emission and absorption lines matches.

The energy of the emitted γ-rays can be decreased by the recoil energy so conservation of energy is satisfied. Similarly, when the photon is absorbed, the absorber recoils back. In the case of atomic transitions, the recoil energies are very small compared to the width of the natural line. Therefore, there is a high probability of absorption of resonance in atomic transitions. In nuclear transitions, resonance absorption is very low.

In the recoil system when increasing the effective mass, the recoil energy decreases. The nucleus transfers energy to the lattice by exciting vibration states by creating phonons. If no phonon is produced, all the energy goes to the emitted photon, which is called

recoilless emission. Figure 1.1 shows the recoilless emission and resonance absorption of γ-rays.

The fraction for non-emission of a phonon is given by the Debye-Waller coefficient, a function in Debye temperature, γ-rays energy and the temperature of both the emitter and the absorber. Because the vibratory excitation process is a quantitative process, there is the possibility of a certain transition that will not transfer any energy into the lattice, that is, the recoilless emission (Philipp Gütlich, 1978).

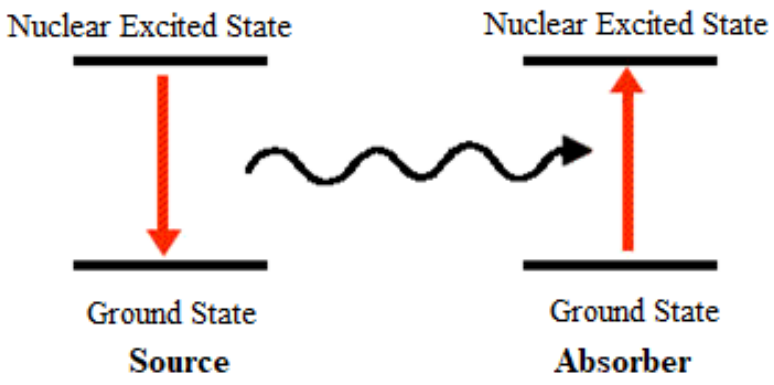

Figure 1.1. Recoilless emission and resonance absorption of γ-rays.

Many isotopes can show Mössbauer effect such as ^{57}Fe, ^{119}Sn, ^{121}Sb and ^{129}I. There are two factors limit the isotopes to be used for Mössbauer spectroscopy namely life time of the excited states and the amount of γ-rays energy (Glaser, 2011).

^{57}Fe isotope is commonly used for Mössbauer spectroscopy. This is because of that large amount of substances used in many applications contain irons. Mössbauer isotopes are shown in figure 1.2.

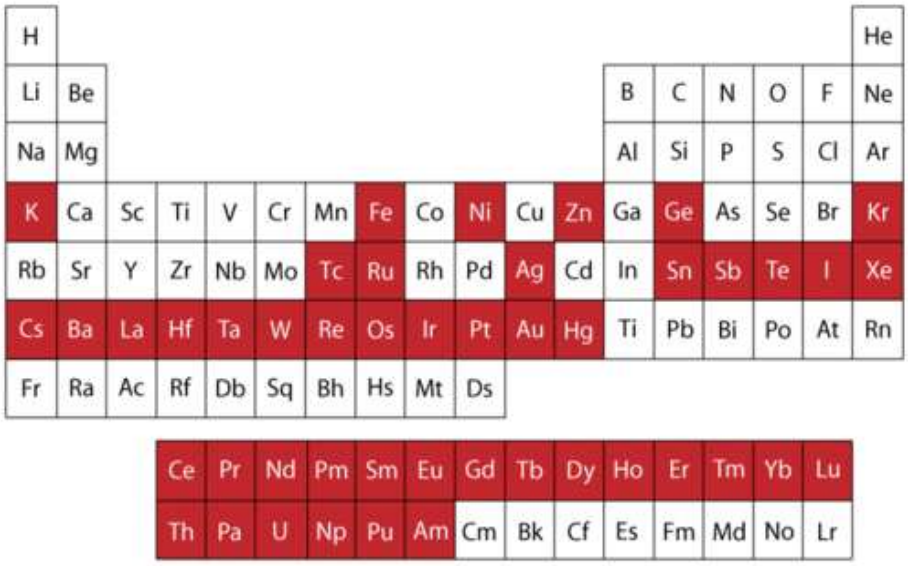

Figure 1.2. Mössbauer isotopes highlighted in red.

1.1.3 Doppler effect

The change in the wavelength or frequency when there is relative motion between the source and absorber is known as Doppler effect. When the source moves toward the absorber, the frequency of waves increases, while the frequency decreases if the source moves away from the absorber (Gill, 1965). Hence the energy of photon is proportional to the relative velocity. By varying the relative velocity of the emitter, it is possible to sweep photon energies over range of values. In Mössbauer spectroscopy, absorption rate is measured as a function of source velocity. Using Doppler effect may covert velocity to energy shift. Analysis of observed absorption peaks reveals details about nuclear energy levels.

1.1.4 Mössbauer applications

Mössbauer spectroscopy becomes powerful tool used in different scientific fields such as in chemistry, physics, biology and geology (Cohen, 2013). The practical application of Mössbauer spectroscopy is not so much concerned with the observation of the effects

itself, but mostly with the effects of the sample's own internal electrical and magnetic fields on the energy of the nuclear states (Greenwood, 2012). It plays significant role in characterizing metal complex by determining oxidation and magnetic state of elements.

For example, this technique has become established for the planetary exploration on the surface of Mars, the presence of water on Mars is confirmed by Mössbauer spectroscopy (Klingelhöfer et al., 2004). Mössbauer spectroscopy was used to solve problems in solid state research (Cohen, 2013). For example it was successfully used to distinguish between Prussian Blue (PB) and Turnbull's Blue (TB). Both these are compounds with the general molecular formula A*x*Ma[Mb(CN)6]zH_2O (where, A is alkali cation, Ma and Mb are metal ion) (Sengupta et al., 2008). Also Mössbauer spectroscopy used to assist in the identification of Fe oxide phases on the basis of their magnetic properties (Lear et al., 1988). Mössbauer spectroscopy is applied to analyses the iron compounds present in car exhausts (Eymery et al., 1978). in geology, Mössbauer spectroscopy can be used to determine redox ratios in rocks (Fleet et al., 2003).

1.1.5 Magnetic materials

Electrons and nuclei have an essential spin, which creates a magnetic moment. These magnetic moments align along in axes. When there is an external magnetic field applied on the materials, the magnetic moments interact with this field. This interaction appear in spin of the electrons, the motion of the electron and the change in motion resulting from the external magnetic field (Cao and Brinker, 2008).

Most of atoms have pair electrons which their spins are in opposite directions because of Pauli Exclusion Principle. As a result, they cancel each other hence, no magnetic field is observed for such atoms. In contrast atoms with unpaired electrons in outer shell are expected to have a magnetic field. Magnetic materials may classify into diamagnetic, paramagnetic, ferromagnetic ferrimagnetic and anti-ferromagnetic. However, in terms of magnetic properties magnetic materials can be either soft or hard. Soft magnetic materials have a low coercivity, whereas hard magnetic materials have a high coercivity (Coey, 2010).

1.1.5.1 Diamagnetic

The orbital motion of electrons in diamagnetic materials generates a field opposite to the external applied field. That is why this type of materials possesses negative magnetic susceptibility. All materials have characteristic of diamagnetism. However, because it is a weak phenomenon other magnetic effects are dominated and hence more observed. (Dorfman, 1965).

1.1.5.2 Paramagnetic

The magnetic state of the paramagnetic materials is due to unpaired electrons. In the absence of an external magnetic applied field the dipole moments of a paramagnetic material are randomly oriented. Therefore, no magnetization effect is observed. The magnetization appears when the magnetic moments aligned by applied magnetic field and then oriented toward same direction of the external magnetic field. (Boudreaux and Mulay, 1976).

1.1.5.3 Ferromagnetic

Ferromagnetic materials exhibit strong interaction between magnetic moments. This appears as spontaneous parallel alignment of magnetic moments. In $T = 0$ the magnetic moment have a perfect alignment. The collapse of ferromagnet order occurs at temperature called Curie temperature T_C (Coey, 2010).

1.1.5.4 Ferrimagnetic

Ferrimagnetism is observed in compounds. The exchange interactions lead to parallel alignment of atoms in some of the crystal sites and anti-parallel alignment of others which leads to magnetization similar to a ferromagnetic material. Ferrimagnet have a Curie temperature T_C and spontaneous magnetization below T_C.

1.1.5.5 Anti-ferromagnetic

In Anti-ferromagnetic materials the exchange interaction between neighbouring atoms leads to anti-parallel alignment of the atomic magnetic moments. Therefore the material

appears to behave in the same way as a paramagnetic material because the magnetic field cancels out. Anti-ferromagnetic materials become paramagnetic above a transition temperature, known as the Néel temperature (Coey, 2010).

1.1.6 Ferrites

A ferrite is a magnetic material that takes the formula MFe_2O_4, which consists mainly of ferric oxides with one or more other metals such as cobalt, manganese and zinc. It has significant saturation magnetization, very good chemical stability and high electrical resistivity. The remarkable properties of ferrite materials make them used in many applications in permanent magnets, cores for transformers, computer memory elements and solid-state devices. Ferrites have three types, namely spinel, cubic garnet and hexagonal ferrites (Division, 1948).

1.1.6.1 Spinel ferrites

Spinel ferrite has a face centered cubic structure with a large unit cell containing eight octants. There are two types of lattices for cation occupancy namely A-site which has tetrahedral and B-site which has octahedral coordination's. M^{+2} and Fe^{+3} cations distribute at both sites. The distribution of the cations over the A and B sites in the spinel can lead to different magnetic properties of these type of oxides even though the chemical composition of the compound does not change (Liu et al., 2000), figure 1.3 show spinel structure.

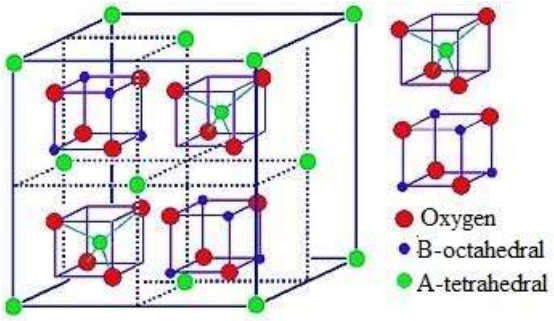

Figure 1.3. Spinel structure, B atoms in octahedral sites and A atoms in octahedral sites, (Liu et al., 2000).

$CoFe_2O_4$ ferrite is a well-known magnetic material with high coercivity, moderate remanence and saturation magnetization, good chemical stability and mechanical hardness (Rao et al., 2015). These properties could make the cobalt ferrite technologically important and has been used in high density magnetic recording media, enhanced memory storage, magnetic fluids and catalysts (Rashad et al., 2008).

$BaFe_2O_4$ ferrite has intrinsic properties such as high chemical stability, low production cost, corrosion resistance high capacity of magnetization, high coercivity and high Curie temperature. These properties have indicated it as a good candidate for microwave devices, radar absorbent materials, permanent magnets, drug deliveries, photo-catalytic catalysts, credit cards (Da Dalt et al., 2011).

1.2 Literature reviews

The measuring temperatures have found to be significantly affecting the magnetic behaviour of spinel ferrite materials. For example, Kazuo Ôno, et al studied the magnetic properties of $FeCl_2$ which were measured over the temperature range of 1.5–530 K. The magnetization was increased while measuring temperature decrease (Ôno et al., 1964). In 2001 P.C. Morais et al investigated the magnetic behaviour of $CoFe_2O_4$ performed at 77 K and 300 K using ^{57}Fe Mössbauer spectroscopy. At 77 and 300 K, the internal field is 489.5 and 423.7 kOe, respectively. The collapsing of the internal field as the temperature increases from 77 to 300 K is explained to be associated with super-paramagnetic behaviour of nano-sized particles (Morais et al., 2001).

Significant microstructure changes may occur due to annealing process. This associated with increase of particle sizes, recovery from structure defects, re-crystallization and phase transformations. Many researchers have studies effect of annealing temperatures on spinel ferrite nanoparticles using Mössbauer spectroscopy.

N.S.E. Osman and T. Moyo and in 2015 present a paper in titled structural and magnetic properties of $CoFe_2O_4$ nanoferrite simultaneously and symmetrically substituted by Mg, Sr and Mn. The magnetic investigation achieved by vibrating sample magnetometer and

Mössbauer spectrometer. However, The Mössbauer measurements of the as prepared $Mg_xSr_xMn_xCo_{1-3x}Fe_2O_4$ nanoferrite series (with x = 0, 0.1, 0.2, 0.3, 1/3) was performed at 300 ^oC (Osman and Moyo, 2015). Annealing temperatures are expected to have a significant influence upon the magnetic behaviour of the synthesized samples. Nevertheless, according to our knowledge, this has not been yet studied.

1.3 Research problem

Thermal treatment can significantly affect the size of particles, hence magnetic behaviour of a material are expected to be changed.

1.4 Research objectives

This work aims to

- Investigate the effect of annealing temperature on magnetic properties of $CoFe_2O_4$ substituted by Mg, Sr and Mn.
- Compare the obtained results of the annealed samples with the reported ones by Osman and Moyo in 2015.
- Study the influence of different measuring temperatures on the magnetic properties of $BaFe_2O_4$.

1.5 Dissertation layout

This dissertation contains four chapters; chapter one gives introduction, literature review and aims of the dissertation. Chapter two describes the theoretical background of Mössbauer spectroscopy. Chapter three shows the experimental details. The results, discussion, conclusions and recommendations are presented in chapter four.

Chapter Two

Theoretical Background

Chapter Two

Theoretical Background

This chapter discusses the theoretical background of Mössbauer spectroscopy. The main idea of Mössbauer spectroscopy measurements is to detect γ-rays that transmitted through the sample under investigation. This associated to the resonant emission and absorption of γ-rays see figure 2.1.

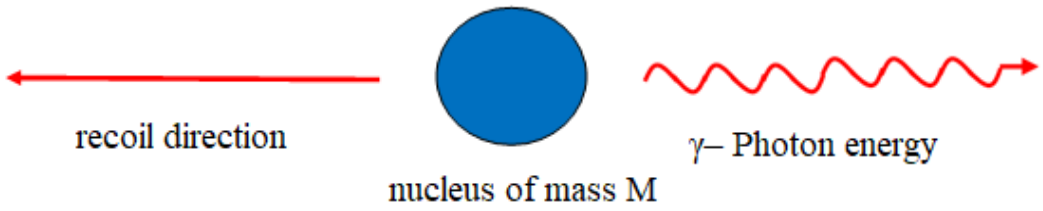

Figure 2.1. Recoil energy loss in free atoms.

The recoil energy E_R is given by

$$E_R = \frac{E_\gamma^2}{2Mc^2}, \qquad 2.1$$

where E_γ is the energy of γ-rays, c is speed of light and M is the mass of the nucleus. *M* has to be replaced by the mass of the entire lattice when Mössbauer source doped in a non-magnetic matrix. This ensures that only a shift in the energy levels of the source occurs without splitting. In ^{57}Fe Mössbauer spectroscopy, the source ^{57}Co isotopes which doped into Rh matrix vibrated in specific way in order to Doppler shift, emitted energy of

γ-rays. This help in matching the energy difference between the excited and ground states. The emitted γ-rays is Doppler shifted by

$$\delta E = \mathrm{E}_{\gamma}\frac{\upsilon}{\mathrm{c}}, \qquad 2.2$$

where υ is the source velocity, δE is energy difference between the excited and ground states.

2.1 Decay of ^{57}Co isotopes

^{57}Co is radioactive source which can decay by electron capture (EC) to I_{ex} = 5/2 of ^{57}Fe isotope. This decay might be directly to the state I_{ex}= 1/2 of ^{57}Fe with probability of 9 %, or it can be to the state I_{ex} = 3/2 with probability of 91%. However, this state (I_{ex} = 3/2) is not stable, hence ^{57}Fe nucleus decay to the ground state by emitting γ-rays with energy of 14.4 keV which related to ^{57}Fe Mössbauer spectroscopy (Lemmer et al., 1955). Figure 2.2 illustrate the nuclear decay of ^{57}Co isotope.

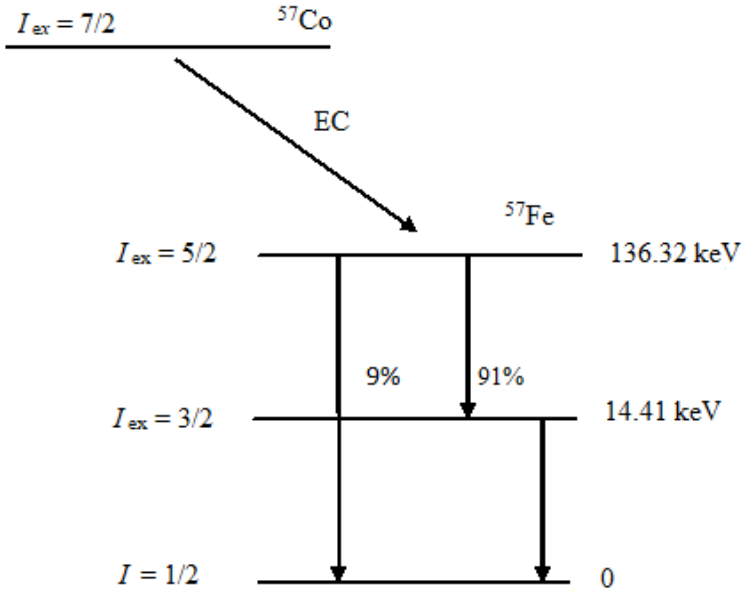

Figure 2.2. Schematic demonstration of ^{57}Co nuclear decay.

2.2 Line width

The transition of ^{57}Fe electrons from the excited to the ground states; the mean life time τ of the excited state cannot be determined exactly because of the limited time interval Δt available for measurements. However, ΔE can be obtained based on Heisenberg uncertainty principle

$$\Delta E.\ \Delta t \geq \hbar, \qquad 2.3$$

where $\Delta t \approx \tau$. However, ground state of infinite life time has zero uncertainty in energy. The natural width of the emission and absorption line can be determined by mean life time τ

$$\Gamma\tau = \hbar, \qquad 2.4$$

Where Γ is line width, $\hbar$ ($\hbar = h/2\pi$) is modified Planck constant 6.582×10^{-16}, $t_{1/2}$ half life time. In ^{57}Fe Mössbauer spectroscopy, the first excited state of ^{57}Fe has mean life time $t_{1/2} = 1.43 \times 10^{-7}$s. The life time values for lower excited nuclear states ranging between 10^{-6} to 10^{-11} seconds (Mössbauer, 1962).

2.3 Recoil-free fraction

The nuclear reactions that occurs without exciting the lattice and cause no change in its quantum state, is known as recoil-free fraction (Malainey, 2011) given by

$$f = exp\left(-\frac{E_\gamma^2 < x^2 >}{(\hbar c)^2}\right), \qquad 2.5$$

2

where $< x^2 >$ is the mean square thermal displacement of the emitting nucleus in the direction of the γ-ray. Based on the Debye model which assumes a range of possible frequencies from zero up to a maximum cut-off frequency, the recoilless fraction can be shown as

$$f = exp\left\{ - \frac{3E_R}{2k_B\theta_D}\left[1 + 4\left(\frac{T}{\theta_D}\right)^2 \int_0^{\frac{\theta_D}{T}} \frac{udu}{e^u - 1}\right]\right\}, \qquad 2.6$$

where k_B is the Boltzmann constant, u =ħω/ (k_BT) and θ_D= ħω$_D$/ k_B is the Debye temperature. Recoil-free fraction is useful to determine the site occupancy (M. D. DYAR, 2008).

2.4 Hyperfine interaction

Hyperfine interaction can be defined as the interaction between nucleus and its environment. In a magnetic environment the energy states of nucleus can split due to an internal magnetic field, this known as Zeeman Effect. Hyperfine interaction gives significant information about magnetic states of a material such as valence state, electron distribution, magnetic order, spin configuration and magnetic relaxation. These information can be obtained experimentally from hyperfine parameters such as isomer shift δ, magnetic hyperfine interaction H and quadrupole splitting Δ.

2.4.1 Isomer shift

Since atoms of source and absorber are in different local environments, their nuclear energy levels are expected to be different, this appears in the transmission spectrum as a shift of the troughs away from zero velocity, known as isomer shift (Da Dalt et al., 2011, Gibb, 1976). This effect usually occurs in radioactive isotopes. The isomer shift reflects the interaction between the nuclear and electronic charges (Gütlich et al., 2011).The coulomb interaction is significantly affected by isomer shift. This because of isomer shift associated with s-electron density due to the changes in the valance electrons. (Filatov, 2009). This causes a shift in nuclear states. Figure 2.3 shows centroid of the Mössbauer spectra that shifted due to isomer shift.

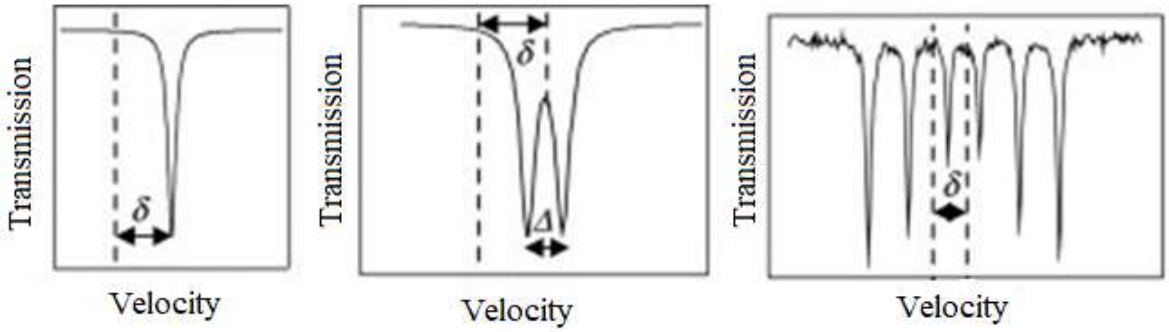

Figure 2.3. Isomer shift in nuclear state.

The isomer shift values can be used to determining valance states, spin state coordination and electron distribution (Neese, 2002). Since this shift cannot be measured directly, it is calibrated to a known absorber. In ^{57}Fe Mössbauer spectra often be calibrated relative to alpha-iron at room temperature (Filatov, 2007). The electron configurations for Fe^{+2} and Fe^{+3} are $3d^6$ and $3d^5$ respectively, the ferrous ions have less s-electron at the nucleus so they have larger positive isomer shifts than ferric ions (Dickson and Berry, 2005). The values of isomer shift for Fe^{+2} ions are in the range of 0.6–1.7 mm/s, whereas for Fe^{+3} ions are 0.1-0.5 mm/s (Gütlich et al., 2011). The isomer shift δ can be calculated using the equation

$$\delta = \Delta E_A - \Delta E_S = \frac{Ze^2}{10\varepsilon_0}[|\psi(0)|_A^2 - |\psi_S(0)|_S^2]\left(R_e^2 - R_g^2\right), \qquad 2.7$$

where E_A and E_S are energy of absorber and sample respectively. Z is the nuclear charge, R_e and R_g are the nuclear radii of ^{57}Fe in the excited and ground state respectively, ε_0 is permittivity of free space. $|\psi(0)|^2$ is electronic charge density.

2.4.2 Magnetic hyperfine interaction

Split of the spectrum in the case of magnetic dipole interaction occurs due to the effect of magnetic field H on the nuclear magnetic dipole moments μ. The magnetic moments is zero in nuclear levels with spin $I = 0$, therefore there is no Zeeman splitting (Jackson and

Hargreaves, 2009). Nuclear levels with spin $I > 0$ has a magnetic dipole interaction give by the Hamiltonian

$$H_d = -\vec{\mu}.\vec{H} = -g_N \mu_N \vec{I}.\vec{H}, \qquad 2.8$$

where g_N is the nuclear landé g-factor, μ_N is the nuclear Bohr magneton. Therefore, the energy levels can be expressed as

$$E_m = -\frac{\mu H m_1}{I} = g_N \mu_N H m_1, \qquad 2.9$$

where m_1 is spin quantum number. The nuclear levels that have spins I are split to $2I+1$ because of the effect of magnetic field. The splitting of the sub-levels is $g_N \mu_N H$, and consists with equal distances. Six possible transitions with selection rules $\Delta m_{1=} 0, \pm 1$caused by Zeeman splitting, appear as sextet in Mössbauer spectrum (Gütlich, 1975). Figure 2.4 show the Zeeman effect in ^{57}Fe.

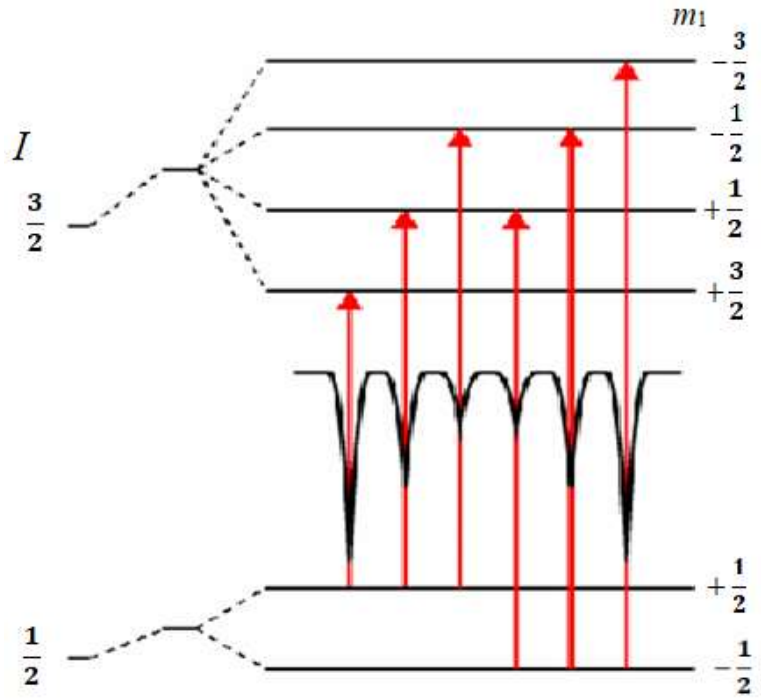

Figure 2.4. Effect of the magnetic dipole interaction in^{57}Fe Mössbauer spectrum.

The magnetic hyperfine fields give information about spin configurations, magnetic moments and magnetic order. In the case of magnetic hyperfine fields as a function of temperatures useful information about magnetic relaxation can be obtained.

2.4.3Quadrupole splitting

A non-spherical nucleus that has a spin quantum number *I* that is greater than 1/2 possess quadrupole moments *Q*. which can be expressed as

$$Q = \frac{1}{e}\int \rho(r)(3z^2 - r^2)dr, \qquad 2.10$$

an asymmetric electric field in the nucleus is produced as a result of asymmetric charge distribution. It is characterized by a tensor quantity called the Electric Field Gradient (EFG). The electric quadrupole interaction between the nuclear moments and EFG gives rise to a splitting in the nuclear energy levels which called quadrupole splitting in Mössbauer spectrum. Quadrupole interaction can be expressed as the Hamiltonian

$$H_Q = \vec{\mathrm{Q}}.\vec{\nabla}E, \qquad 2.11$$

the eigenvalues of the last equation are given by

$$E_Q = \frac{eQV_{ZZ}}{4I(2I-1)}\left(3m_I^2 - I(I+1)\right)\left(1+\frac{\eta^2}{3}\right)^{\frac{1}{2}}, \qquad 2.12$$

where $V_{ZZ} = \partial V/\partial Z^2$ is the principle axis component of the electrical field gradient, m_I is the magnetic quantum number and η is an asymmetry parameter of the electric field given by

$$\eta = \frac{V_{zz} - V_{yy}}{V_{zz}}, \qquad 0 \le \eta \le 1 \qquad 2.13$$

Due to quadrupole interaction the excited state $m_I = 3/2$ of ^{57}Fe isotope splits while the ground state $I = 1/2$ remains unsplit because of lack of quadrupole moments. Double

generate sub states create from splitting of the excited state due to m_I^2 dependence of the quadrupole energies

$$E_Q\,(\pm 3/2) = 3eQV_{zz}/12, \qquad 2.14$$

$$E_Q\,(\pm 1/2) = -3eQV_{zz}/12\,, \qquad 2.15$$

The transition from I = 3/2 to I = 1/2 appears as a doublet in the Mössbauer spectrum which is separated by quadrupole splitting given by

$$\Delta E_Q = E_Q\,(\pm 3/2) - E_Q\,(\pm 1/2) = \frac{eQV_{zz}}{2}. \qquad 2.16$$

Quadrupole splitting provides information about charge distribution, defects and charge symmetry around the nucleus of a sample (Dickson and Berry, 2005). Figure 2.5 shows splitting in Mössbauer spectrum due to the effect of electric quadrupole interaction.

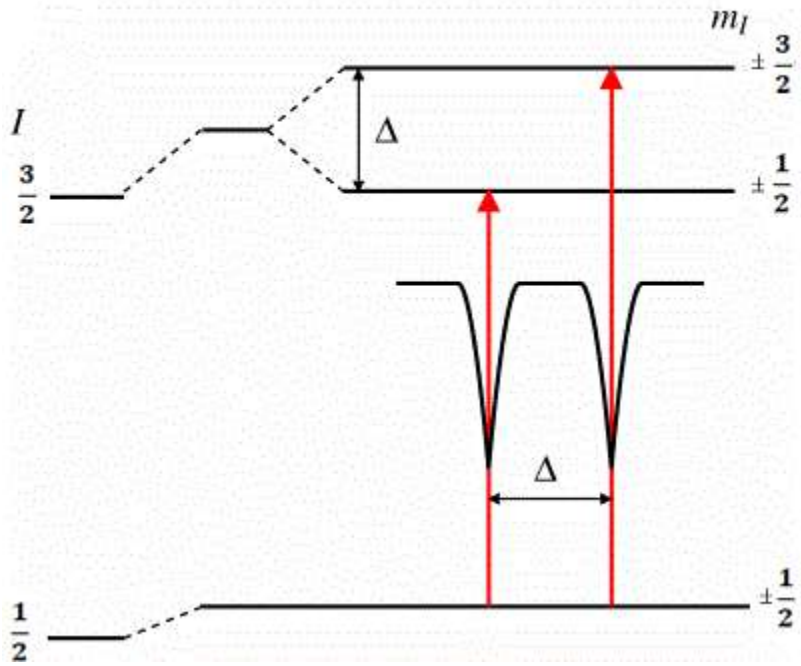

Figure 2.5. Effect of the electric quadrupole interaction leads to splitting in Mössbauer spectrum.

Chapter Three

Experimental Details

Chapter Three

Experimental Details

3.1 Introduction

This chapter provides a discussion about experimental technique of Mössbauer spectroscopy that was used in this work. Mössbauer spectrometer consists of several parts namely drive system, γ-rays source, absorber and detector.

In ^{57}Fe Mössbauer spectroscopy, the radioactive source ^{57}Co is used which first decays to the excited state of ^{57}Fe then subsequently decays to its ground state giving γ-rays with energy 14.4 keV. The resonance takes place when energy of emitted γ-rays equals the energy difference of ^{57}Fe levels in the absorber. This may occur by moving the γ-rays source leading to Doppler effect. Thus the γ-rays source is connected to an electromechanical velocity transformer, also known as Mössbauer drive system which powered by electronic drive control unit provided by the digital function generator. The detector converts the γ-rays into electrical pulses. This process involves device such as pre-amplifier, main amplifier and a single-channel analyzer (SCA). The SCA is a pulse recognition device which can be tuned to a Mössbauer radiation filter such that pulses of resonance energy passes into the multi-channel analyzer (MCA) for acquisition, and rejects all pulses from unwanted non-resonant background radiation. The MCA is the central device for Mössbauer spectra for data acquisition and storage. It consists of a set of digital counters to separate electrical pulses. The collected Mössbauer spectrum is recorded on a computer screen.

3.2 Mössbauer drive system

Mössbauer spectrometer often works in continuous acceleration mode, where the velocity drive is pulled up and down and the source periodically moves back and forth by two ways either saw-tooth or triangular mode. The Mössbauer electromechanical transducer, can change the velocity range from 1 mm/s to several cm/s. The primary frequency of the drive motion must be adjusted before the first resonance of the

mechanical unit, which usually in range of 10–30 Hz. The frequency determines the recurrence rate of the Mössbauer measurement by the motion of source up and down in the whole velocity scale for spectra cumulating until the end of the measurement. The amplitude of the velocity range is selected by calibration the reference voltage (VR) at the drive control unit. The quality of the velocity control can be tuned by setting the characteristics of the feedback loop. The actual efficiency of the transducer can be seen from the size of the so-called error signal, which is the voltage difference at the inputs (VR) and (V_{resp}) of the difference amplifier of the drive control unit. The error signal can be observed with an oscilloscope connected to output In order to optimize the performance, the corresponding dials on the front panel of the control unit can be adjusted to minimize the error signal while observing the oscilloscope.

3.3 The Mössbauer source

The resonance absorption takes place when the emitted γ-rays from the nucleus of the source isotope can be detected in the sample, which is usually a stable isotope. To obtain such nuclei for γ-emission in the source, a long-living radioactive parent isotope is used, the decay of which passes through the Mössbauer level. Mössbauer's sources are technically prepared by diffusing radioactive material into a matrix of non-magnetic metal with a cubic crystal lattice. The acquisition of narrow Mössbauer emission lines without a hyperfine splitting division requires that the matrix does not impose a magnetic moment and does not include an electric field for the source nucleus.

3.4 Mössbauer detector

Mössbauer detector converts γ-photons into electrical pulses. The detection process of γ-photons by the Mössbauer detector must be energy-sensitive to distinguish γ-lines from other radiations. Therefore, the detector is preferred to have a high sensitivity to γ-radiation. This also protects electronic components from unnecessary load. The mentioned features of Mössbauer detector helps to achieve count quickly with strong pulses and high count rates.

3.5 Recording the Mössbauer spectrum

To collect a Mössbauer spectrum, the electric pulses must be recorded synchronously by the γ-rays detection system by sweep the source velocity. This can be achieved by operating the MCA in the so-called multichannel scaling (MCS) mode, in which the function generator triggers the digital counters (channels) of the MCA sequentially, one by one. The channels collect incoming γ-ray pulses by increasing the value of digital storage. The memory is initialized when it receives a start pulse from the function generator at the trigger input (T). The start pulse is synchronized with the sweep reference voltage (VR) for the Mössbauer drive. It opens the first MCA channel when the source velocity is at minimum. After this start trigger, a set of "channel progress" pulses follow a precise delay time of approximately 100 ms. when the pulse is received, MCA closes the open channel and open the next one, which opens to record γ-pulses. When the last channel is closed, the MCA is reset and ready to start the next cycle. The process is repeated with a spectra frequency of 20 Hz per cycle velocity until the measurement is stopped. Through this step the channels are opened sequentially and closed for identical corresponding times, which in total match the velocity sweep period. Thus, γ-recording is synchronized with the source movement so that each counting channel corresponds to a different increase of the velocity range. The counters stored in each channel of the Mössbauer spectrometer given the channel number as a function of the Doppler velocity. Typical formation times for such Mössbauer spectrum may range from several hours to several days, depending on iron concentration and absorption thickness. After measurement, the content of the MCA memory is transferred to a computer and stored as an array of N numbers for further processing and analysis, where N is the number of channels used to record the spectrum. Any change of the spectrometer velocity setting requires recording of a new calibration spectrum. The calibration of the energy scale of a Mössbauer spectrometer is a primary step of data analysis. The simplest way is to use the spectrum of a standard absorber with known hyperfine splitting. Figure 3.1 shows schematic diagrammatic of a Mössbauer spectrometer.

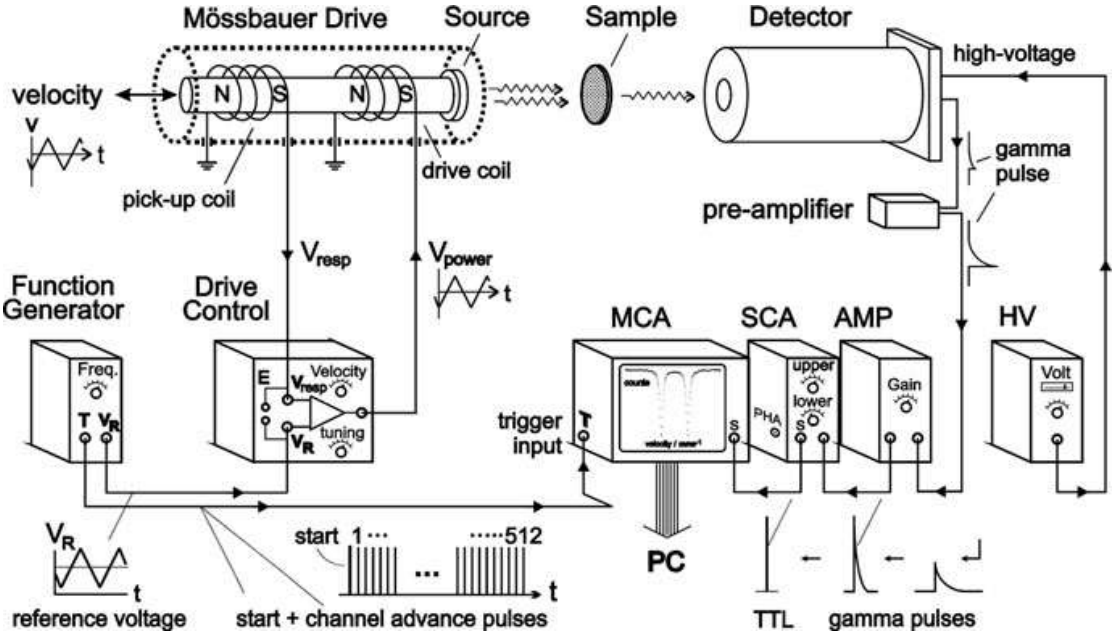

Figure 3.1. Schematic diagrammatic of Mössbauer spectrometer, (Gütlich et al., 2011).

3.6 Mössbauer measurement procedures for the studied samples

^{57}Fe Mössbauer spectra for the studied samples were obtained by a conventional spectrometer using a ^{57}Co source sealed in Rh matrix and vibrated at constant acceleration of 12 mm/s. A 0.11 g of the sample was spreaded out into a non magnetic sample holder and then placed between the ^{57}Co source and sodium iodide detector. Mössbauer measurements of each sample were achieved for 24 hour. For the annealed samples of $Mg_xSr_xMn_xCo_{1-3x}Fe_2O_4$ (x = 0, 0.1, 0.2, 0.3, 0.33) nanoferrites the measurements was achieved at room temperature. While Mössbauer spectra for $BaFe_2O_4$ was measured at different temperatures of 77, 80, 90, 160, 200, 250 and 300 K. The temperature was monitored by lakeshore model-735 temperature controller as shown in figure 3.2.

Figure 3.2. Mössbauer spectrometer cryostat, Condensed Matter Physics Laboratory, Westville Campus, South Africa.

Figure 3.3. Front setup of Mössbauer spectrometer, Condensed Matter Physics Laboratory, Westville Campus, South Africa.

Chapter Four

Results and Discussion

Chapter Four

Result and Dissection

4.1 Introduction

This chapter discusses the obtained Mössbauer results for the annealed samples of $Mg_xSr_xMn_xCo_{1-3x}Fe_2O_4$ (x = 0, 0.1, 0.2, 0.3, 0.33). The discussion extends to analysis the temperature dependence of Mössbauer results for $BaFe_2O_4$. The discussion includes the values of isomer shift, magnetic hyperfine field, line width and *f*-fraction.

4.2 Magnetic properties of the annealed $Mg_xSr_xMn_xCo_{1-3x}Fe_2O_4$ nanoparticles ferrites

Mössbauer measurements for $Mg_xSr_xMn_xCo_{1-3x}Fe_2O_4$ (x = 0, 0.1, 0.2, 0.3, 0.33) samples annealed at 500 ^oC were performed at room temperature. As shown in figure 4.1, two sextets were used to fit the obtained spectra. Each sextet corresponds to Fe^{3+} ions in ordered spin state that distributed on tetrahedral A-site and octahedral B-site (Rao et al., 2015). This is attributed to Zeeman effect which indicate ferrimagnetic behaviour of the compounds. However, A doublet was needed to obtains a better fit for the sample of x = 0.33. The need for the doublet is noticed to be associated with disappearing of Co ions. This is considered to be as indication to paramagnetic state of the sample. The results obtained from room temperature Mössbauer measurements are presented in table 4.1. Large values of hyperfine field in octahedral site are due to the covalent nature of the Fe_2O_4 bonds due to spread Fe^{3+} ions without existence of other elements in this site (Msomi et al., 2016). As shown in figure 4.2, magnetic hyperfine field values of $Mg_xSr_xMn_xCo_{1-3x}$ Fe_2O_4 (x = 0, 0.1, 0.2, 0.3, 0.33) annealed at 500 ^oC are higher compared to as-prepared samples reported by N.S.E. Osman (Osman et al., 2013). Since temperature treatment can increase particle sizes of a sample (Iqbal et al., 2008) , Therefore, larger values of the annealed sample in figure 4.2 can be attributed to the increase in particle sizes which associated with decrease in relaxation time (Msomi et al.,

2016). The relaxation rate τ is related to particle's volume V and anisotropy energy density K by Néel's equation (Jing et al., 1990)

$$\tau^{-1} = \tau_0^{-1} \exp\left(-\frac{KV}{k_B T}\right), \quad 4.1$$

Where $\tau_0$is (10^{-9} – 10^{-10}s) is the inverse of the natural frequency of the gyro-magnetic precession, T is temperature in K and k_B is the Boltzmann constant. Néel's relaxation associated with the redirection of the magnetic moments within the particles. The bond separation Fe^{3+} □ O^{2-} in cubic spinel ferrites is expected to be larger at octahedral site compared to that at tetrahedral site. This is because of small overlapping of Fe^{3+} ions orbital. Therefore, isomer shift values at octahedral site are expected (see table 4.1). Slightly difference has been observed between isomer shift values for the annealed samples and the as prepared ones as reported in (Osman et al., 2013). This reflects that the s-electrons charge distribution of Fe^{3+} ions has not been significantly affected by the annealing process. It is known that isomer shift values for Fe^{3+} lie in the range 0.1-0.5 mm/s and for Fe^{+2} are in the range 0.6-1.7 mm/s (Philipp Gütlich, 1978). Thus the results obtained for the annealed samples show only presence of Fe^{3+} ions. Line width values decreases in annealed samples. This is expected because of the increase of magnetic hyperfine field leads to more sharpness of the Mössbauer sextets. The values of *f*-fraction reflect the distribution of Fe^{3+} in tetrahedral and octahedral sites of the investigated samples (Sawatzky et al., 1969). Hyperfine parameters are significantly affected by annealing temperature.

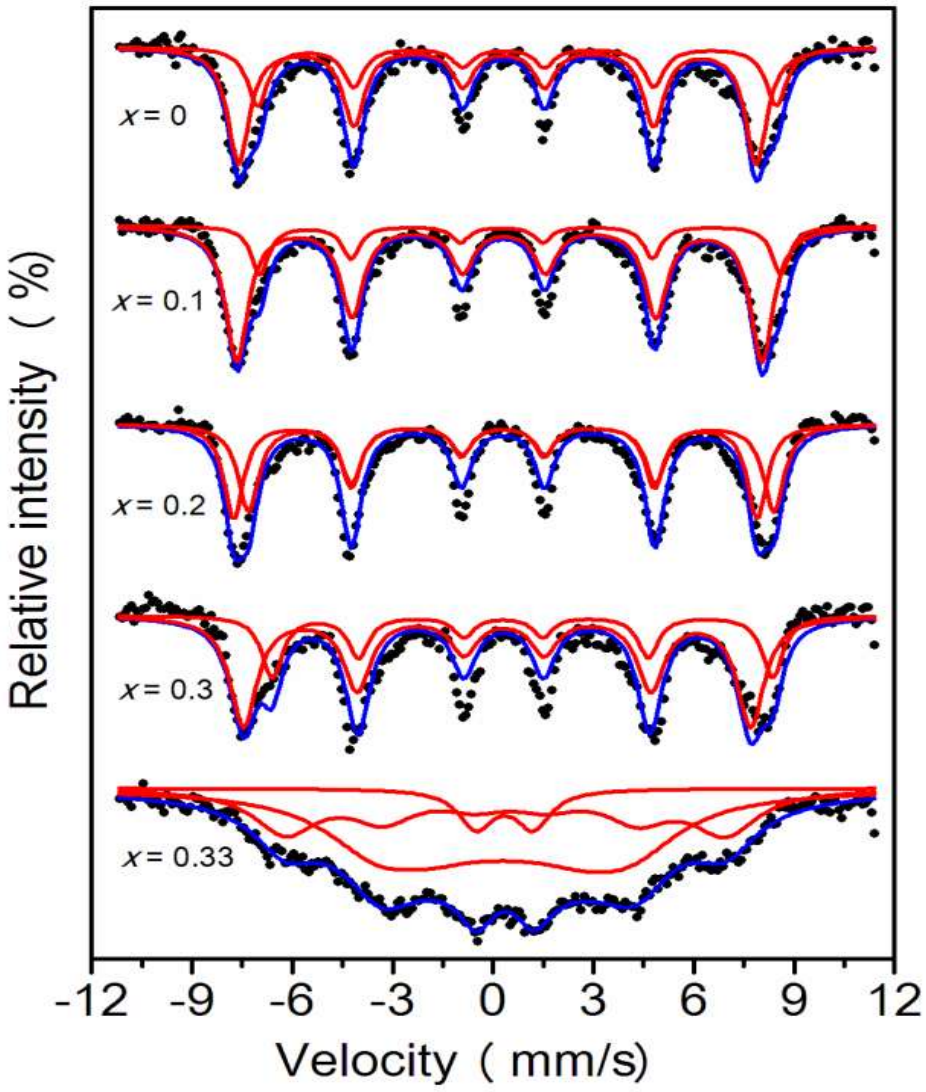

Figure 4.1. Mössbauer spectra for $Mg_xSr_xMn_xCo_{1-3x}Fe_2O_4$ nanoferite samples annealed at 500 ^oC.

Table 4.1. Isomer shifts (δ), hyperfine magnetic fields (H), line widths (Γ) and Fe^{+3} fraction population (f) on A- and B- sites for $Mg_xSr_xMn_xCo_{1-3x}Fe_2O_4$ samples annealed at 500 °C.

X	δ (mm/s)		H (kOe)		Γ (mm/s)		f (%)	
	δ_A	δ_B	H_A	H_B	Γ_A	Γ_B	f_A	f_B
	±0.7	±0.9	±4	±3	±1.4	±0.6	±3	±3
0	0.28	0.30	449	486	0.33	0.21	46	53
0.1	0.28	0.51	483	498	0.25	0.17	74	25
0.2	0.28	0.30	462	494	0.36	0.12	60	39
0.3	0.34	0.33	435	484	0.48	0.21	62	37
0.33	0.29	0.31	228	412	1.32	0.56	53	33

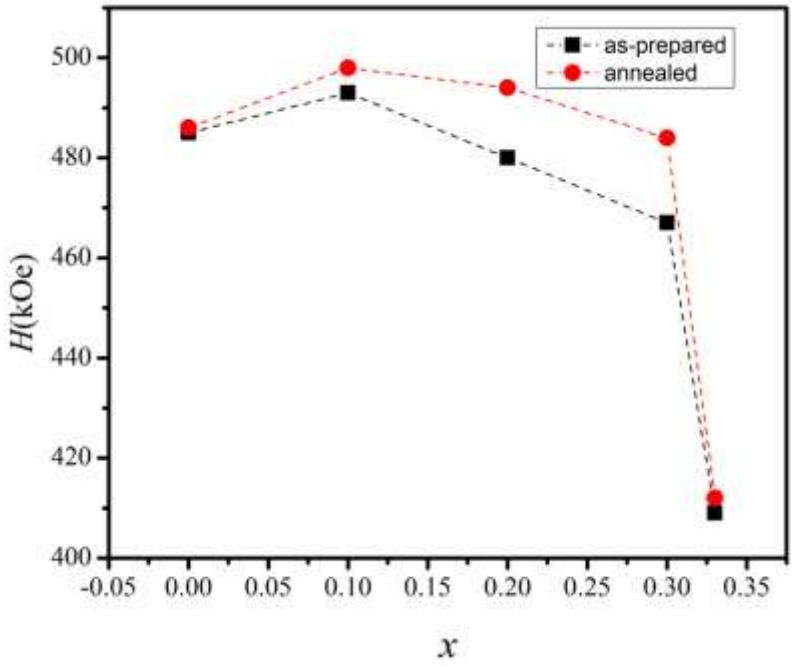

Figure 4.2. Magnetic hyperfine fields values of $Mg_xSr_xMn_xCo_{1-3x}Fe_2O_4$ (x = 0, 0.1, 0.2, 0.3, 0.33) annealed at 500 °C compared to as-prepared sample.

4.3 Analysis of Mössbauer spectra for $BaFe_2O_4$ sample as a function of measuring temperatures

Mössbauer measurements for $BaFe_2O_4$ sample were performed at different temperatures of 77, 80, 90, 160, 200, 250 and 300 K. The obtained Mössbauer spectra are shown in figure 4.3. Two sextets were used to fit the sample at measuring temperatures of 77, 80 and 90 K whilst, two doublets were used to fit the sample at measuring temperatures of 200, 250 and 300 K. Two sextets and doublet were used to obtain better fitting for the sample measured at 160 K. This expected to be due to presence of both the ferromagnetic and paramagnetic phases in the sample. Mössbauer spectra changed from sextet to doublet above 160 K. The sextet with the higher hyperfine field is attributed to Fe^{3+} ions without Ba^{2+} in their neighbourhood lattice. The second sextet with lower hyperfine field is due to Fe^{3+} ions with Ba^{+2} neighbours. The two doublets that were used to fit the sample at measuring temperatures of 200, 250 and 300 K are associated with Obsession of Ba^{2+} ions which indicates to paramagnetic state (Raevski et al., 2018). The obtained results are presented in table 4.2. The magnetic hyperfine field values decrease as measuring temperature increases (see figure 4.4). The variation of magnetic hyperfine fields is due to the effect of measuring temperature on magnetic order of the material. Similar behaviour were noticed by (Long and Grandjean, 2013). The results conclude that the ferromagnetic order of $BaFe_2O_4$ sample changed to paramagnetic state. This effect may explained by Curie temperature (Murad and Cashion, 2011). Curie temperature is the critical temperature when the magnetization of material reveals from ferromagnetic to paramagnetic transition (Mohan et al., 1998). The orbital overlapping of Fe^{3+} on B site is smaller compared to A site, thus, the bond separation is expected to be larger at B site. Therefore, the values of the isomer shift of $BaFe_2O_4$ sample are expected to be larger at B site compared to A site. Furthermore, the obtained isomer shift values are in the range 0.20 to 0.45 mm/s. This are associated with Fe^{3+} ions as reported in reference (Kurian, 2011). Line width values appear to be influenced by increasing the measuring temperatures reflecting the change of magnetic order of the sample. The maximum line

width broadening is found for the sample at measuring temperature of 200 K. *f*-fraction shows the distribution of Fe^{3+} in tetrahedral and octahedral sites (Sawatzky et al., 1969).

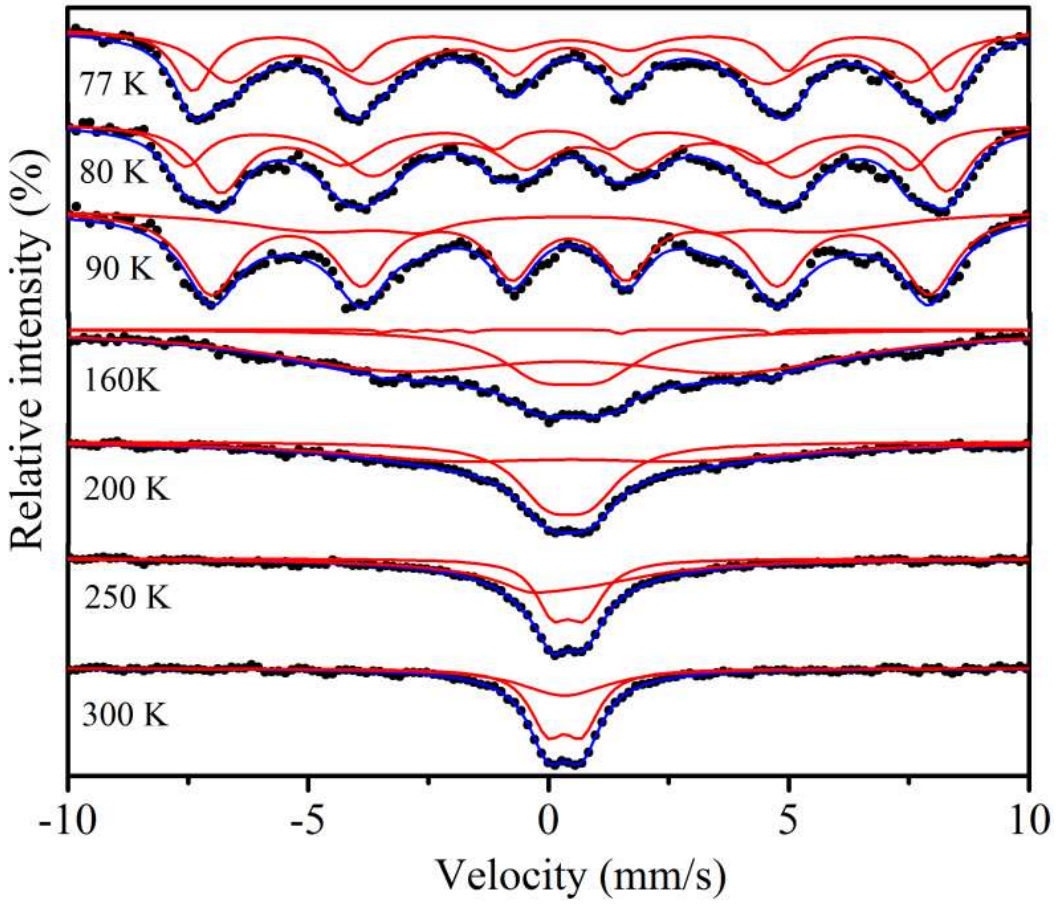

Figure 4.3. Mössbauer spectra as a function of measuring temperature for $BaFe_2O_4$ sample.

Table 4.2. Isomer shifts (δ), hyperfine magnetic fields (H), line widths (Γ) and Fe^{+3}fraction population (f) on A- and B- sites for $BaFe_2O_4$ as a function of measuring temperature.

T(K)	δ (mm/s)		H (kOe)		Γ (mm/s)		f (%)	
	δ_A	δ_B	H_A	H_B	Γ_A	Γ_B	f_A	f_B
	±0.07	±0.03	±3.6	±1.1	±0.07	±0.06	±3	±3
77	0.45	0.45	440	486	0.50	0.74	62.8	37.1
80	0.34	0.41	467	468	0.69	0.40	53.2	46.7
90	0.41	0.44	323	463	2.40	0.57	26.8	73.1
160	0.30	0.26	047	099	2.80	0.10	73.6	0.74
200	0.40	0.44	-	-	0.77	2.80	45.7	54.2
250	0.41	0.38	-	-	0.43	2.20	26.0	73.9
300	0.33	0.33	-	-	1.10	0.43	38.1	61.4

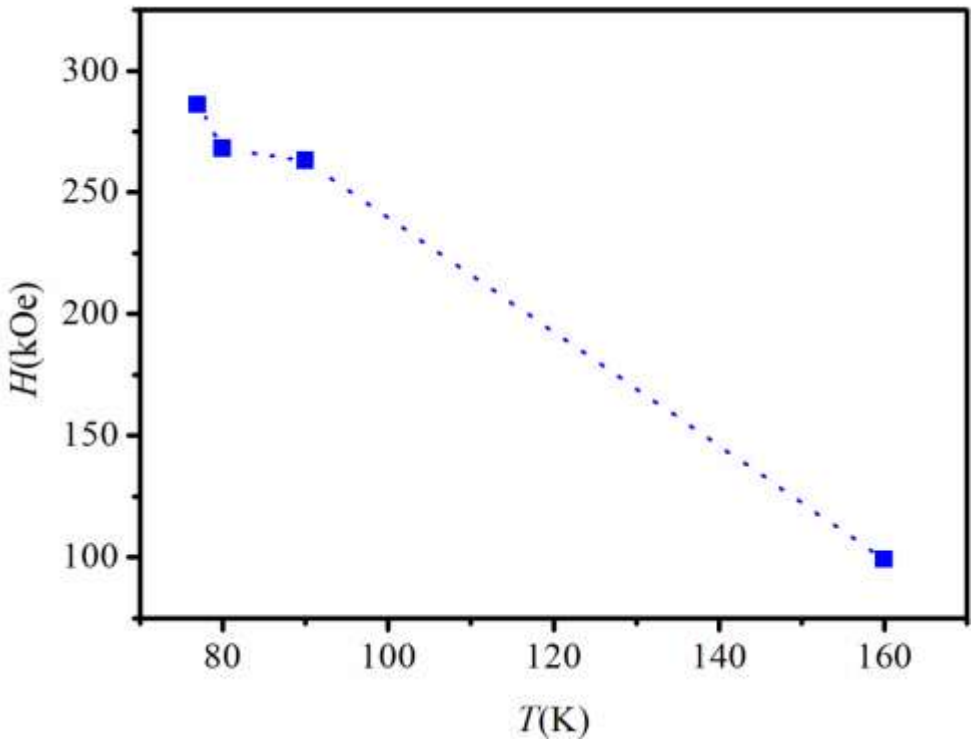

Figure 4.4. Magnetic hyperfine fields as a function of measuring temperature.

4.3 Conclusions

Mössbauer spectroscopy have been studied and applied for more than 50 years and are considered as well-known technique that used to study magnetic properties of materials. Particularly, ^{57}Fe Mössbauer spectroscopy considered to be one of the most important techniques in investigating magnetic properties of ferrite materials. Investigation of magnetic properties of the annealed nanoparticles ferrites at 500 ^{o}C show that the hyperfine magnetic fields of the annealed samples were larger compared to the as prepared samples. This can be attributed to the increase in particle sizes. Isomer shift increased while line width decreased. Thermal annealing shows significant affects on the magnetic properties of the studied samples. Investigation of magnetic properties of $BaFe_2O_4$ sample at different temperatures of 77, 80, 90, 160, 200, 250 and 300 K were successfully achieved. The results show that magnetic hyperfine fields decreased as measuring temperatures increase. The values of isomer shift in the range of 0.45-0.2 mm/s. Line width and *f*-fraction were also affected by measuring temperatures. The effect of annealing and measuring temperature on $Mg_xSr_xMn_xCo_{1-3x}Fe_2O_4$ and $BaFe_2O_4$, respectively were successfully investigated using ^{57}Fe Mössbauer spectroscopy. The results show that temperature treatment has significant influence in magnetic properties of the studied samples.

4.4 Recommendations

- Study quadruple splitting for the investigated samples. This will give information about charge distribution, defects and charge symmetry around the nucleus of a sample.

- Increasing the particle sizes due to annealing temperature for the investigated samples can be precisely monitored using X-rays diffraction technique.

4.5 Future Work

The followings can be suggested as a future work:

- Study the effect of different annealing temperatures on magnetic properties of $Mg_xSr_xMn_xCo_{1-3x}Fe_2O_4$ nanoparticles.

- Study the effect of annealing temperature on magnetic properties of $BaFe_2O_4$ sample.
- Study the effect of higher measuring temperature (beyond 300 K) on magnetic properties of $BaFe_2O_4$.

References

BOUDREAUX, E. A. & MULAY, L. N. 1976. Theory and applications of molecular paramagnetism, Wiley.

CAO, G. & BRINKER, C. J. 2008. Annual Review of Nano Research, World Scientific.

COEY, J. M. 2010. Magnetism and magnetic materials, Cambridge University Press.

COHEN, R. L. 2013. Applications of Mössbauer spectroscopy, Academic Press.

DA DALT, S., SOUSA, B. B., ALVES, A. K. & BERGMANN, C. P. 2011. Structural and photocatalytic characterization of BaFe2O4 obtained at low temperatures. Materials Research, 14, 505-507.

DICKSON, D. P. & BERRY, F. J. 2005. Mössbauer spectroscopy, Cambridge University Press.

DIVISION, U. S. A. F. A. M. C. D. 1948. Technical Data Digest, Air Documents Division, Intelligence T-2, Air Matériel Command.

DORFMAN, I. A. G. 1965. Diamagnetism and the Chemical Bond, American Elsevier Publishing Company.

EYMERY, J. P., RAJU, S. B. & MOINE, P. 1978. The application of Mössbauer spectroscopy in investigating iron compounds in car exhaust. Journal of Physics D: Applied Physics, 11, 2147.

FILATOV, M. 2007. On the calculation of Mössbauer isomer shift. The Journal of Chemical Physics, 127, 084101.

FILATOV, M. 2009. First principles calculation of Mössbauer isomer shift. Coordination Chemistry Reviews, 253, 594-605.

FLEET, M. E., DEER, W. A., HOWIE, R. A. & ZUSSMAN, J. 2003. Rock-forming Minerals: Micas, Geological Society.

GIBB, T. C. 1976. Hyperfine Interactions. Principles of Mössbauer Spectroscopy. Boston, MA: Springer US.

GILL, T. P. 1965. The Doppler effect: an introduction to the theory of the effect, Logos Press.

GLASER, T. 2011. Mössbauer Spectroscopy and Transition Metal Chemistry. Fundamentals and Applications. Edited by Philipp Gütlich, Eckhard Bill and Alfred X. Trautwein. Angewandte Chemie International Edition, 50, 10019-10020.

GREENWOOD, N. N. 2012. Mössbauer spectroscopy, Springer Science & Business Media.

GUTLICH, P. 1975. Mössbauer spectroscopy in chemistry. In: GONSER, U. (ed.) Mössbauer Spectroscopy. Berlin, Heidelberg: Springer Berlin Heidelberg.

GUTLICH, P., BILL, E. & TRAUTWEIN, A. X. 2011. Mössbauer-Active Transition Metals Other than Iron. Mössbauer Spectroscopy and Transition Metal Chemistry: Fundamentals and Applications. Berlin, Heidelberg: Springer Berlin Heidelberg.

IQBAL, M., ALI, S. & MIRZA, M. 2008. Effect of particle size on the structural and transport properties of $La_{0.67}$ $Ca_{0.33}$ MNO_3 nanoparticles. Journal of Natural Sciences and Mathematics, 48, 51-63.

JACKSON, S. D. & HARGREAVES, J. S. J. 2009. Metal Oxide Catalysis, Wiley.

JING, J., ZHAO, F., YANG, X. & GONSER, U. 1990. Magnetic relaxation in nanocrystalline iron-oxides. Hyperfine Interactions, 54, 571-575.

KAKKAR, R. 2015. Atomic and Molecular Spectroscopy: Basic Concepts and Applications, Cambridge, Cambridge University Press.

KLINGELHöFER, G., MORRIS, R. V., BERNHARDT, B., SCHRöDER, C., RODIONOV, D. S., DE SOUZA, P., YEN, A., GELLERT, R., EVLANOV, E. & ZUBKOV, B. 2004. Jarosite and hematite at Meridiani Planum from Opportunity's Mössbauer spectrometer. Science, 306, 1740-1745.

KURIAN, R. 2011. First Principles Theoretical Modeling of the Isomer Shift of Mössbauer Spectra, University Library Groningen][Host].

LEAR, P. R., KOMADEL, P. & STUCKI, J. W. 1988. Mössbauer spectroscopic identification of iron oxides in nontronite from Hohen Hagen, Federal Republic of Germany. Clays Clay Miner, 36, 376-378.

LEMMER, H. R., SEGAERT, O. J. A. & GRACE, M. A. 1955. The Decay of Cobalt 57. Proceedings of the Physical Society. Section A, 68, 701.

LIU, C., ZOU, B., RONDINONE, A. J. & ZHANG, Z. J. 2000. Chemical Control of Superparamagnetic Properties of Magnesium and Cobalt Spinel Ferrite Nanoparticles through Atomic Level Magnetic Couplings. Journal of the American Chemical Society, 122, 6263-6267.

LONG, G. J. & GRANDJEAN, F. 2013. Mössbauer Spectroscopy Applied to Magnetism and Materials Science, Springer US.

M. D. DYAR, M. W. S., E. C. SKLUTE , J. L. BISHOP 2008. Mo□ssbauer spectroscopy of phyllosilicates: effects of fitting models on recoil-free fractions and redox ratios. Clay Minerals, 43, 3-33.

MALAINEY, M. E. 2011. Mössbauer Spectroscopy. A Consumer's Guide to Archaeological Science: Analytical Techniques. New York, NY: Springer New York.

MOHAN, C. V., SEEGER, M., KRONMULLER, H., MURUGARAJ, P. & MAIER, J. 1998. Critical behaviour near the ferromagnetic–paramagnetic phase transition in La0. 8Sr0. 2MnO3. Journal of magnetism and magnetic materials, 183, 348-355.

MORAIS, P. C., GARG, V. K., OLIVEIRA, A. C., SILVA, L. P., AZEVEDO, R. B., SILVA, A. M. L. & LIMA, E. C. D. 2001. Synthesis and characterization of size-controlled cobalt-ferrite-based ionic ferrofluids. Journal of Magnetism and Magnetic Materials, 225, 37-40.

MöSSBAUER, R. L. 1962. Recoilless Nuclear Resonance Absorption of Gamma Radiation. Science, 137, 731-738.

MSOMI, J., NDLOVU, B., MOYO, T. & OSMAN, N. 2016. Mössbauer and magnetic properties of annealed $Ni_xCo_{1-x}Fe_2O_4$ nanoparticles. Journal of Alloys and Compounds, 683, 149-156.

MURAD, E. & CASHION, J. 2011. Mössbauer spectroscopy of environmental materials and their industrial utilization, Springer Science & Business Media.

NEESE, F. 2002. Prediction and interpretation of the ^{57}Fe isomer shift in Mössbauer spectra by density functional theory. Inorganica Chimica Acta, 337, 181-192.

ÔNO, K., ITO, A. & FUJITA, T. 1964. The Mössbauer Study of the Ferrous Ion in $FeCl_2$. Journal of the Physical Society of Japan, 19, 2119-2126.

OSMAN, N., MOYO, T. & ABDALLAH, H. 2013. Synthesis and magnetic investigation of $Mg_xSr_xMn_xCo_{1-3x}Fe_2O_4$ nanoparticle ferrites.

OSMAN, N. S. & MOYO, T. 2015. Structural and magnetic properties of $CoFe_2O_4$ nanoferrite simultaneously and symmetrically substituted by Mg, Sr and Mn. Materials Chemistry and Physics, 164, 138-144.

PHILIPP GUTLICH, E. B. L. A. X., TRAUTWEIN 1978. Mössbauer Spectroscopy and Transition Metal Chemistry, London New York.

RAEVSKI, I. P., KUBRIN, S. P., PUSHKAREV, A. V., OLEKHNOVICH, N. M., RADYUSH, Y. V., TITOV, V. V., MALITSKAYA, M. A., RAEVSKAYA, S. I. & CHEN, H. 2018. The effect of Cr substitution for Fe on the structure and magnetic properties of $BiFeO_3$ multiferroic. Ferroelectrics, 525, 1-10.

RAO, K. S., CHOUDARY, G. S. V. R. K., RAO, K. H. & SUJATHA, C. 2015. Structural and Magnetic Properties of Ultrafine $CoFe_2O_4$ Nanoparticles. Procedia Materials Science, 10, 19-27.

RASHAD, M., MOHAMED, R. & EL-SHALL, H. 2008. Magnetic properties of nanocrystalline Sm-substituted $CoFe_2O_4$ synthesized by citrate precursor method. Journal of Materials Processing Technology, 198, 139-146.

SAWATZKY, G. A., VAN DER WOUDE, F. & MORRISH, A. H. 1969. Recoilless-Fraction Ratios for ^{57}Fe in Octahedral and Tetrahedral Sites of a Spinel and a Garnet. Physical Review, 183, 383-386.

SENGUPTA, P., SAIKIA, P. C. & BORTHAKUR, P. C. 2008. SEM-EDX characterization of an iron-rich kaolinite clay. J Scien Ind Res, 67, 812-818.